Journal of Applied Electrochemistry (2022) 52:17–33
https://doi.org/10.1007/s10800-021-01618-1

RESEARCH ARTICLE

Fabrication of titanium nanotubes array: phase structure, hydrophilic properties, and electrochemical behavior approach

Amal M. Abdel-Karim[1] · **Sahar A. Fadlallah**[2]

Received: 29 April 2021 / Accepted: 9 August 2021 / Published online: 23 August 2021

Abstract

Surface modification of Ti is the point of interest to researchers due to its promising biomedical applications, especially in bone replacement surgery. In the current work, a new bioactive (Ti) implant surface was prepared for possible dental and orthopedic applications by anodization and heat treatment. Ti was anodized at sequential potential periods in NH_4F/glycerol bath at different glycerol concentrations and, then annealed to form crystalline TiO_2 nanotube, labeled (cry TNT). Then the (cry TNT) was dipped in 0.29 g l^{-1} $CaCl_2$ solution to diffuse Ca^{2+} ions into its infrastructure. The phase, morphology, and chemical composition of the prepared surface modified with/or without Ca^{2+} ions were examined with X-ray diffraction (XRD), scanning electron microscopy (SEM) and energy dispersive X-ray (EDX) analysis. The bioactive stability of the surface was investigated via electrochemical impedance spectroscopy (EIS) in simulated body fluid solution (SBF) to investigate the effect of incorporation of Ca^{2+} ions to induce hydroxyapatite-like structure via the fitting process. In conclusion, 10% cry TNT surface with pore size 43 nm was found to bind to Ca^{2+} ions from the bulk solution to fill its pores resulting in an increase in the resistance from 78 to 118 kΩ. The produced new bioactive surface with its high hydrophilic properties represents a promising approach to design and fabricate innovative surfaces with high bonding ability for dental and orthopedic applications.

✉ Amal M. Abdel-Karim
amalabdelkarim720@gmail.com

[1] Physical Chemistry Department, National Research Centre, 33 El Bohouth St., Dokki, Giza 12622, Egypt

[2] Chemistry Department, Faculty of Science, Cairo University, Giza 12613, Egypt

Graphic abstract

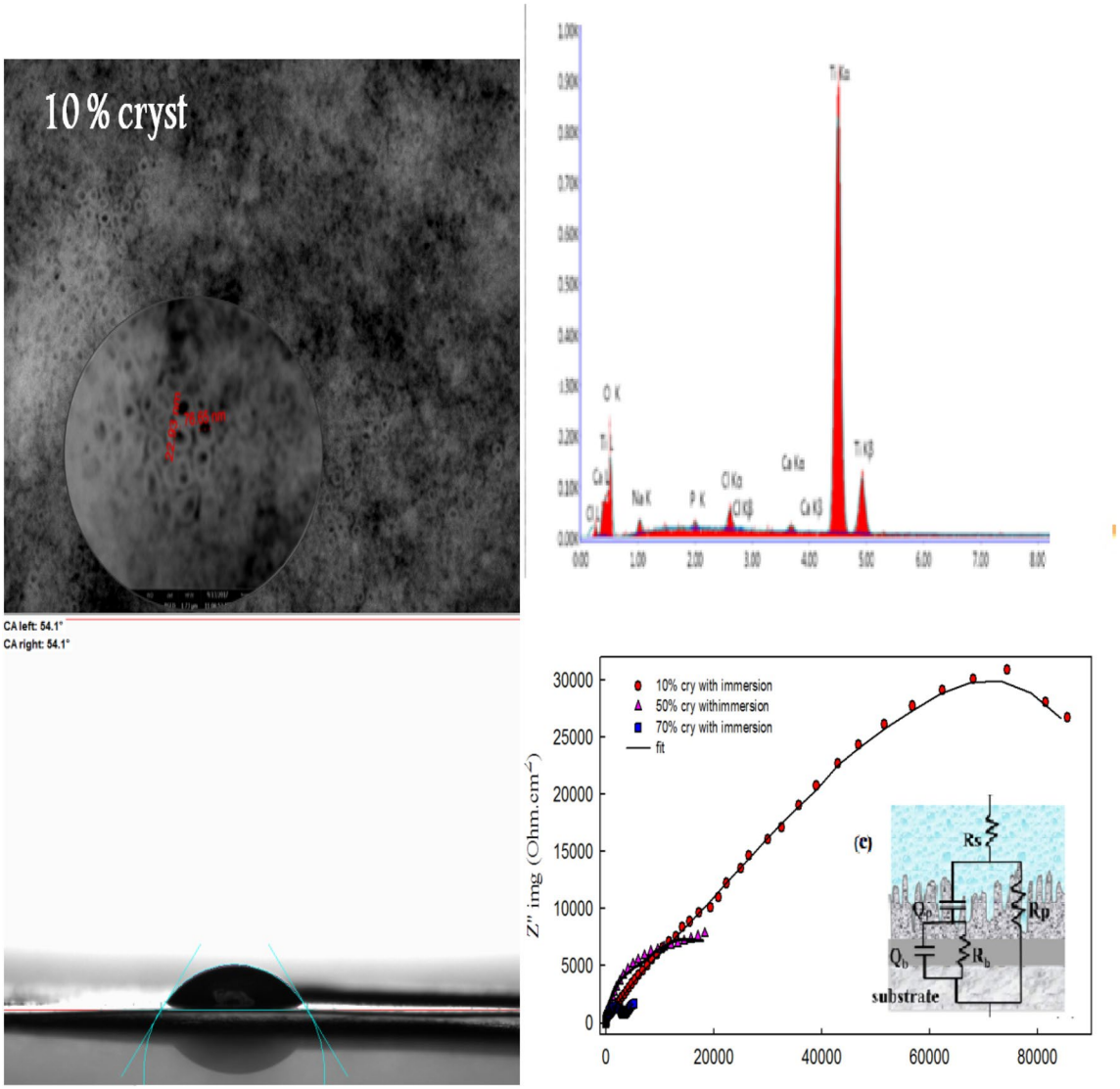

Keywords Anodization · Titanium nanotubes TNTs · Anatase TiO_2 · Hydrophilic · Calcium ion loading ability · SBF · Electrochemical impedance

1 Introduction

During the past years, traditional metal surfaces as stainless steel in bone replacement and mercury amalgam as dental implants have proved to have many health hazardous effects, besides the possible need for re-operation of the implant more than one time [1]. This urges more efforts to develop new biomaterials for medical implants, which accelerates normal wound healing phenomena. Pure titanium and its alloys have been used as implants due to their low density, lightweight, corrosion resistance, and biocompatibility [2]. Protective native TiO_2 layer is spontaneously formed in the air on the Ti surface raising its corrosion resistance in physiological medium, yet this amorphous layer is not sufficient to bond strongly with bone tissues, which usually leads to early failure after surgeries because of the weak nature of the bound bones rendering them more easily fractured [3–5].

Extensive research is devoted to possible surface Ti modifications to improve bone deposition and in turn aids shorter healing period [6]. These modifications depend on changing the properties that influence the biological interaction at the bone-implant interface including pore size, thickness, crystallinity, wettability [7, 8], and alloying elements [9–13]

The anodization process is a simple electrochemical tool, over the other physical and chemical surface modifications techniques, that has been broadly applied to modify the surface and promote its integration at the solid–liquid interface [14, 15]. Using aqueous and non-aqueous electrolytes without or with fluoride ions plays an important role in improving titanium layers to accommodate different applications.

Based on the literature, many methods are presented for the preparation of TiO_2 nanorods [16] nanowires [17], and nanotubes [18–20] through electrochemical anodization [21, 22]. Among these reported methods, anodization proved to be a simple rendering ordered TiO_2 nanotubes arrays on Ti surface. Different electrolytes like H_2SO_4–HF [23], neutral electrolytes Na_2SO_4–NaF [24], and ethylene glycol-NH_4F [25] have already been used to form TiO_2 nanotubes. Therefore, it is of great importance to correlate between the composition and concentration of the electrolytes and the properties and the behavior of titanium surfaces [26, 27].

As the surfaces with strong hydrophilic properties can easily bind to water molecules and solutes, and adsorb macromolecules from the medium as proteins through electrostatic adsorption, while preserving their structure which facilitates their interaction with bone tissue cells. Therefore, the hydrophilic improvement of Ti surfaces was the objective of many electrochemical processes [28, 29]. Bone tissues grown on porous Ti surfaces with good wettability led to good adhesion and osteogenic marker production [30–33]. Also the pore-size nanoscale surface topography < 100 nm can significantly enhance cell adhesion [32] spreading [33] and also increase alkaline phosphatase activity [34].

Typically, electrolyte nature optimizations at different pH, temperature, anodization potential, or current and heat treatments are performed to monitor the structure, crystallinity, and properties of nano-porous layers such as porous diameter, wall thickness, and surface roughness. Moreover, ion incorporation into the porous structure of the implant surface plays an additional role to develop the biological responses. Calcium and/or phosphorous ion implantations modify surface chemistry and bioactivity both in vitro and in vivo [35]. Particularly, calcium ions are implanted by dynamic ion mixing to induce a strong bond between the apatite film and the titanium substrate [36] and serve as a binder to accelerate calcium phosphate precipitation on the implant surface [37]. Usually, anodized TiO_2 (Titania) has an amorphous structure, but after heat treatment, it crystallizes into the anatase phase or a mix of anatase and rutile phases at 600 °C [38]. Phase changes affect both surface properties of nanostructure and bioactive reactions. Therefore, understanding the relationship between TiO_2 nanostructures features and their bioactivity is essential for planning and preparing the suitable implant surface. Although several publications on porous TiO_2 nanostructures investigated their properties and applications, only a few studied the connection between the concentration of the anodizing solution and the size of pores, and the hydrophilic properties of the formed Titania.

This work aims to fabricate the new nanotubes Titania surfaces (TNTs) by double anodization/ annealing of titanium under sequential potential periods in NH_4F/glycerol bath at different glycerol concentrations (10, 50, and 70%) and track their electrochemical behavior by EIS measurements. Morphology, chemical composition, pore sizes, and phase of the Titania (TiO_2) layers were analyzed by SEM/EDX analysis and XRD. The contact angle was measured to elucidate the wettability of the surfaces at different glycerol concentrations. The bioactivity of the surfaces filled with/and without Ca^{2+} ions was estimated through EIS measurements in SBF solution over an extended period at human body temperature 37 °C and pH 7.4.

2 Experimental

2.1 Fabrication of samples

Titanium foils (2.50 mm thick, 97%, Sigma-Aldrich, Chemie GmbH, Riedtr.2D-89555 Steinheim 49 7329-970, Germany) with a size of 1×2.5 cm were polished with P320, P600, P1200, and P2400 grade SiC emery paper and then cleaned with deionized water, ethanol and acetone in an ultrasonic bath for 10 min and dried using compressed air, prior to performing the upcoming steps.

2.1.1 Anodization

Potentiostatic anodization process occurs in the two-electrode electrochemical cell at room temperature in two steps; the first involves three potential values (5 then 10 then 15 V) with anodization time of 20 min at each potential; the second step includes two potential values (20 then 30 V) for 1 h at each potential. 0.84 wt% NH_4F and different concentrations (10, 50, and 70%) of glycerol were used as an anodizing electrolyte. Subsequently, the formed amorphous samples were rinsed with water, then with acetone, and finally air-dried.

2.1.2 Heat-treatment

The amorphous samples after anodization were annealed in 6000 Furnace thermolyne at the heating rate of 10 °C per 1 min at 450 °C for 1.5 h, and at 650 °C for 1.5 h, to change the amorphous phase into an ordered crystalline phase which was verified by XRD analysis and coded as 10, 50 and 70% (cry TNTs).

2.2 Surface examination

The morphology, chemical composition, and the pore size of the samples with/or without immersion in Ca^{2+} ions were studied using high resolution scanning electron microscope JEOL-JSM-5600. The surface was covered with a 30-nm-thick gold film formed by sputtering on the anodized specimens to make the surface electrically conductive. The anodic film's chemical composition was measured with energy-dispersive x-ray spectroscopy EDX at 10 kV accelerating potential. During the EDX study, a relatively low accelerating potential was used to further limit the interaction volume of electrons in Titania film and to extract a piece of complete surface information. EDX were used to test the Ca/P ratio on surfaces.

2.3 XRD analysis

The crystalline phases of TNTs before and after heat treatment with/or without Ca^{2+} ions were performed by X-ray diffraction provided with a computer-controlled X-ray diffractometer formally made by PHILIPS-MPD X PERT equipped with Cu radiation Cu K_α ($K = 1.54056$ A). The x-ray tube used was a copper tube operating at 40 kV and 30 mA. The scanning range was 20° to 80° (2θ) with a step size of 0.02° and counting times of 35/step. Quartz was used as the standard material to correct for the instrumental broadening. The degree of crystallography (d) was also calculated using the Scherer equation [39].

$$d = \frac{k\lambda}{\beta \cos\theta}, \tag{1}$$

where d is the crystallite size, k is a constant depends on the shape with the value close to unity (equal to 0.9), λ wavelength of X-rays, and β is the full width at half maximum (FWHM) for (111) reflection, the value of β is radians reflecting the line broadening at FWHM is equal to 2θ axis of diffraction, θ is the Bragg's angle.

2.4 Surface wettability

Surface wettability of titanium substrate, 10%, 50%, and 70% cry TNT and 10% with immersion in Ca^{2+} ions were investigated by (OCA 15EC) contact angle produced by the company of Data Physics Instrument, 70794 Filderstadt, Germany. A droplet of de-ionized water was mounted on the Titania film surface using a micro-syringe. For a fixed volume of the drop, a curvature profile was created and the contact angle was measured. The average values of the contact angle were calculated from at least 3 individual measurements taken at different locations on the surface.

2.5 Electrochemical measurements

The electrochemical impedance spectroscopy (EIS) was achieved using Workstation Metrohm autolab potentiostat/galvanostat version PGSTAT 302N. A three-electrode cell was used which include, Pt as a counter electrode, Ag/AgCl as a reference electrode while 10%, 50%, or 70% cry TNTs were used as the working electrodes. Simulated body fluid (SBF) consisting of NaCl (8.00 g l^{-1}), $NaHCO_3$ (0.36 g l^{-1}), $NaHPO_4{\cdot}2H_2O$ (0.06 g l^{-1}), KCl (0.4 g l^{-1}), KH_2PO_4 (0.4 g l^{-1}), and Glucose (1 g l^{-1}) pH 7.4 at 37 °C [40] was used as an electrolyte. EIS spectra were obtained at an open circuit potential, with ac voltage amplitude of 10 mV and a scan frequency range of 0.01 Hz–10^5 Hz. The samples were soaked in a naturally aerated SBF test solution for different durations extended up to 7 days. The EIS spectra were simulated using the Nova software 1.11. To clarify the effect of Ca^{2+} ions, the samples of 10%, 50%, and 70% cry TNTs were immersed in a 0.29 g $l^{-1}Ca^{2+}$ solution for 6 h before measurements compared to the samples without immersion. The real impedance Z' and imaginary Z'' are calculated from Z in the equation

$$Z = Z'(\omega) + Z''(\omega), \tag{2}$$

where ω is the angular frequency ($\omega = 2\pi f$), f is the frequency. The EIS was plotted in the form of Nyquist.

3 Results and discussions

The activity of the prepared titanium oxide nanotube (TNT) was evaluated by its interaction with the SBF buffer with and without Ca^{2+} ions. Amorphous titanium oxide was prepared in different concentrations of glycerol in the presence of fluoride ion under applied potential then annealed to give crystalline titanium oxide (cry TNT). Different features were described including morphology, chemical composition, pore sizes, phase structure, and wettability of all new surfaces under different conditions.

3.1 Surface characteristics

3.1.1 Morphology

In general, the electrochemical conditions including anodized potential, anodizing time, and concentration of electrolyte are the most important factors controlling the formation of a well-ordered nanotubes structure. Two simultaneous processes occur in fluoride solution first, anodized potential

assisted oxidation of Ti to Titania and assisted dissolution of Ti metal ions in the solution, finally, chemical dissolution of Ti and TiO_2 in presence of hydrogen and fluoride ions occurs.

The HR-SEM images of the top view of the fabricated 10%, 50%, and 70% cry TNTs without immersion in Ca^{2+} ions are shown in Fig. 1. The well-separated nanostructures with cleared gray and dark gray organized pores can be noticed. The average diameter and wall thickness of nanotubes are listed in Table 1.

As seen from the results, the glycerol concentration plays an important role in controlling the porosity of the fabricated film. The average diameter of cry TNT without Ca^{2+} ions was found to be arranged descending as 76.65, 59.90, and 52.45 nm while the wall thickness is arranged in ascending order of 22.93, 33.56, and 40.20 nm for 10%, 50%, and 70% respectively.

These results indicate that the samples formed with a lower concentration of glycerol yielded larger pore size and thinner wall thickness. Schmuki et al. [41] found that, the increase in pore size and decrease in wall thickness can be attributed to the pronounced effect of more oxide dissolution [42, 43]. This result confirms that the mechanism of the nanotubes TiO_2 layer formed on the Ti surface depended on the migration of Ti^{4+} at the oxide/metal interface that reacts with O^{2-} and OH^- through the formation of Ti–O bond. On increasing the anodizing potential, these bonds become weak which allowing more O^{2-} ions to diffuse from the bulk solutions into the electrode surface to form thicker oxide layers with the nanotubes structure [43].

The presence of the fluoride ions in the solution increases the dissolution/diffusion process resulting in the promotion of nanostructure planning of the oxide layers and stronger adhesion [44–46]. As the glycerol concentration rises, the number of Ti^{4+} ions at the anode increase leading to an increase in the oxide film thickness [7]. The diameters of the nanotubes were found to be more uniform for 10% glycerol than in the case of using 50% and 70% glycerol. This indicated that the concentration of glycerol plays a part in the distribution of the size homogeneity of the resulting nanotubes. Figure 2 represents the morphology of the fabricated 10%, 50%, and 70% (cry TNTs) after immersion for 6 h in SBF containing 2.9 g l^{-1} Ca^{2+}.

The average pore diameter of TNT with Ca^{2+} ions is 43.27 nm, 46.17 nm, and 56.11 nm ordered in an ascending order with oxide walls of 32.46 nm, 25.96 nm, and 18.45 nm for 10%, 50%, and 70% respectively. Accordingly, it can be concluded that the pore size decreases in the presence of Ca^{2+} that confirming the diffusion from the bulk solution into the inner surface of the tube.

As shown in Fig. 2 the pores size of 10% TNT immersed in Ca^{2+} was found to reduce faster than the pores size of the 50% and 70%TNTs, where Ca^{2+} ions filled the holes of the 10% in 6 h immersion. This result is in agreement with that previously reported by Liang et al. [47].

3.1.2 Chemical composition and phase analysis

The presence of Ti and oxygen in the EDX analysis clearly confirmed the chemical structure of 10%, 50%, and 70% cry TNT without Ca^{2+} ions as shown in Fig. 1. It is obvious that TiO_2 was formed at the surface of the three samples [48].

Figure 3 and Table 2 represent the EDX analysis of 10, 50, and 70% cry TNTs immersed in Ca^{2+} for 6 h. The appearance of both Ca and P signals in addition to the Ti and O peaks refers to the enhancement of their deposition as a result of anodization and temperature treatments [49]. The outcome of this experiment revealed that the 10% cry TNT could integrate calcium and phosphorous ions into the nanolayer at a ratio (1.3). Thus the oxide film on this particular sample is promising to be used as a human body-compatible substance [50]. But the percent of Ca and P was noticed on the 50% and 70% samples, may lead to bad biocompatible behavior for these surfaces as will be shown later.

Upon increasing the immersion time to 7 days in SBF containing Ca^{2+} for the 10% cry TNT sample, a marked oxide growth was observed resulting in an observable development of oxide layer as seen in Fig. 4. It is seen that a thick precipitated layer from the Ca/P was formed at a ratio of 1.47 which is very close to the normal Ca/P ratio of 1.67.

In general, calcium-ion implantation into a 10% cry TNT surface improves the bioactivity of this sample via increasing the apatite-inducing ability [51–53] as will be examined electrochemically in the following sections by evaluating the stability of the passive films.

Additionally, the phase-type of 10% TNTs before and after heat treatment with/and without calcium ions was examined and validated by XRD measurements as shown in Fig. 5, which predicted that the prepared nanostructures are amorphous before heat treatment [54] but may also include certain crystalline phases, depending on anodization potential [55].

The XRD patterns for the 10% amp TiO_2 samples without and with Ca^{2+} ions are coded A1 and A2, respectively, while those for the 10% cry TNT samples without and with Ca^{2+} ions coded C1 and C2, respectively. As expected, wide broad diffraction peaks are pointed to the amorphous samples, while anatase or a mixture of anatase and rutile with low broad diffraction peaks were depicted for samples calcined at 450° C and 650 °C [56]. The XRD pattern revealed that a low-intensity broad peak centered at around $2\theta = 25.45°$ for the samples A1 and A2. This is a typical peak of brookite TiO_2, therefore suggesting low crystallinity of the oxide films. In addition, small and broad XRD peaks of amorphous TNTs were recorded. Dikici et al., observed the formation of a small proportion of anatase and rutile phases of TiO_2

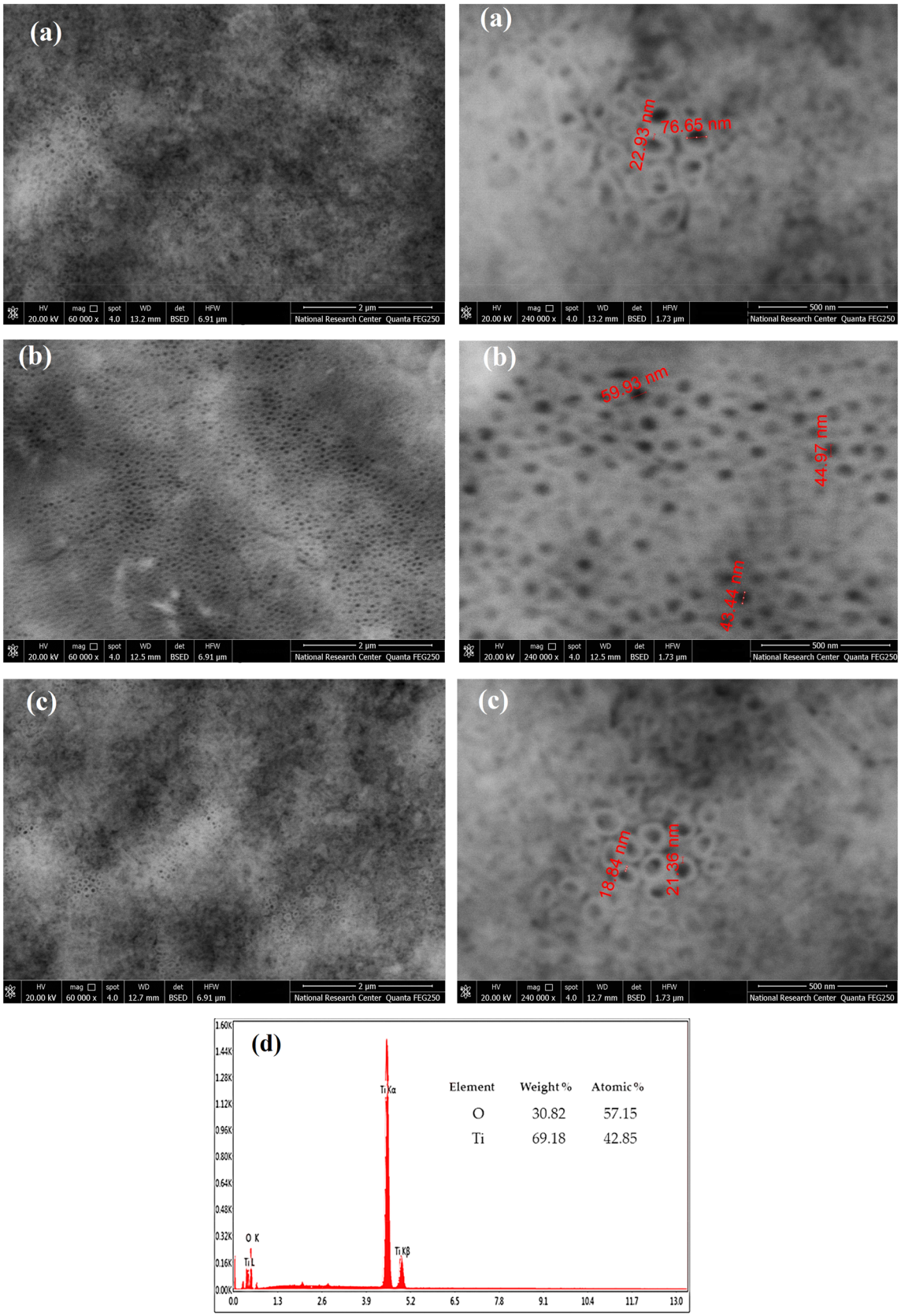

Fig. 1 HR- SEM images of anodized /annealed samples **a** 10%, **b** 50%, and **c** 70% cry TNTs without immersion in $Ca^{2+}$and **d** EDX analysis

Table 1 Pore size and wall thickness of Cry TNTs with /and without immersion in Ca^{2+} ions from SEM images

Glycerol concentration (%)	Ca^{2+} ions immersion	Pore diameter (nm)	Wall thickness (nm)
10	Without	76.65	22.93
	With	43.27	32.46
50	Without	59.90	33.56
	With	46.17	25.96
70	Without	52.45	40.20
	With	56.11	18.45

along with bulk amorphous phase during titanium anodization carried out at 20 V in 1 wt% HF at room temperature [57]. XRD pattern for cry TNTs C1 and C2, displayed the metallic titanium peaks at $2\theta = 38°$, 40.4° and 53.2°, respectively [58]. The other peaks are found at 2θ values of 25.34°, 38.79°,48.0°, 54°, 55.88°, 62.85°, 70°, 74°, and 75°, are attributed to the anatase TiO_2 (JCPDS card no. 21-1272). On the other hand, the diffraction peaks of the rutile phase are found at $2\theta = 27.42°$, 35.88°, and 55.84°, respectively [41]. The development of crystalline titanium oxides under anodic oxide thin film deposition conditions has been previously reported [37, 38].

The intensity of anatase titanium dioxide peaks increased during annealing, which indicated that crystallinity is in turn increased, and the wall thickness of annealing samples with immersion in Ca^{2+} was 32.46 nm higher than 22.9 nm in case of samples measured without immersion in Ca^{2+} solution, which facilitates the nucleation of crystalline TNTs.

The XRD patterns for the samples immersed in Ca^{2+} ions have the same diffraction peaks of untreated samples, and extra peaks found at $2\theta = 31°$, 32°, 43° and 82° due to the presence of adsorbed ions such as Ca and P ions for A2 and C2 samples. This result implies that the porous anatase nanotubes fashioned on the surface of titanium enhance calcium and phosphorus flow in simulated body fluid [18, 35].

Additionally, the grain sizes of these samples, estimated from the Scherrer equation, are 57, 50, 47, and 41 nm for A1, A2, C1, and C2 samples, respectively. Thus, it is clear that the grain size of the anodized sample is larger than the anodized/annealed one.

3.1.3 Wettability

The surface wettability of the 10, 50, and 70% cry TNTs in comparison with the Ti substrate were estimated through contact angle measurement as shown in Fig. 6a–f. It is found that, the values of contact angles are 81.7°, 66. 5°, 108.2°, and 110.1° for Ti substrate, 10, 50, and 70% cry TNTs, respectively. Although, 10% amorphous Titania has a contact angle equal to 67.9° close to the cry TNT 66.5°, a significant decrease in the contact angle to 54.1° is observed for 10% cry TNT filled with Ca^{2+} ions sample after immersion in Ca^{2+} for 6 h. This result refers to the key role of Ca^{2+} ion in increasing the hydrophilic properties. In other words, the change in wetting behavior of the surfaces is attributed to the well-separated arrays formed with 10% concentration, that significantly enhance the surface properties of the film from hydrophobic 50% and 70% cry TNT to hydrophilic 10% cry TNT and this change is enhanced by Ca^{2+} diffusion.

This agrees with the previous findings that confirm the nano-network layer known as anatase TiO_2 [8] can reduce the contact between the surface with the surrounding tissue by improving the hydrophilicity, which greatly affects *in-vivo* cell responses [59]. It is clear, that the anatase phase is the most efficient phase for enhanced wettability and the breakdown in the nanostructure frame due to dissolution which is responsible for the reduction of the liquid distribution inside the nanotubes leading to an increase in water droplet arch [60] which in turn increase the contact angles. In addition, the increase of contact angles is attributed to the shrinkage of the pore diameter as seen in Table 1. Therefore, the hydrophilic surface is preferable to greater protein adsorption and Ca^{2+}, which enhances cellular behavior compared with a hydrophobic surface.

In the next section, the effect of the four parameters (pore size, grain size, Ca^{2+} ions implantation, and contact angle) will be related to the electrochemical behavior of cry TNT samples to deduce the corrosion resistance of this sample in SBF.

3.2 Electrochemical behavior

3.2.1 OCP measurements

Figure 7a, b shows the variation of open circuit potential (OCP) with time for10, 50, and 70% cry TNTs in the simulated solution SBF without/and with Ca^{2+} ions at 37 °C and pH 7.4. For all anodized electrodes, the OCP decreases with time for the first minutes of immersion and slowly all curves reached almost constant states. The data of the initial OCP values, illustrated the effect of Ca^{2+} ions enhancing the initial stability of all samples by shifting the potential to more positive values − 160 to − 69 mV for 10% cry TNT, − 100 to − 90 mV for 50% cry TNT and − 115 to − 78 mV for 70% cry TNT as shown in Table 3.

10% cry TNT without Ca^{2+} ions is initially − 160 mV, but after more than one day of immersion, the stability of the surface increases by the potential shift to a more positive value − 115 mV, this shift can be due to the relative stability of the formed passive films on Ti surface. While the OCP of 10% cry TNT after immersion in Ca^{2+} ions was initially − 69 mV, and then shifted towards the negative potential region after 2 days of immersion in

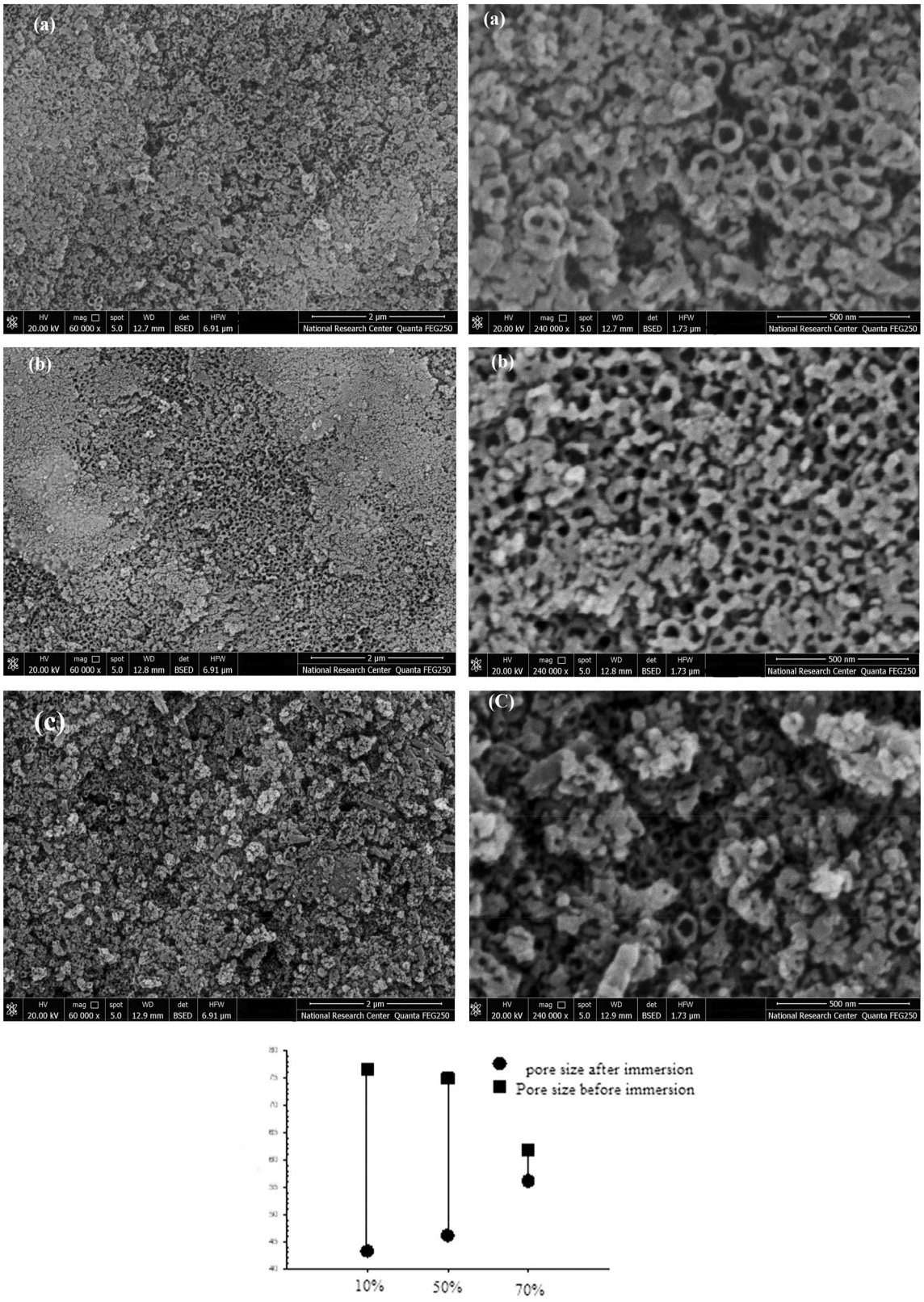

Fig. 2 SEM images and pore size of anodized /annealed samples **a** 10%, **b** 50% and **c** 70% cry TNT after immersion in 0.29 g l^{-1} Ca^{2+} for 6 h

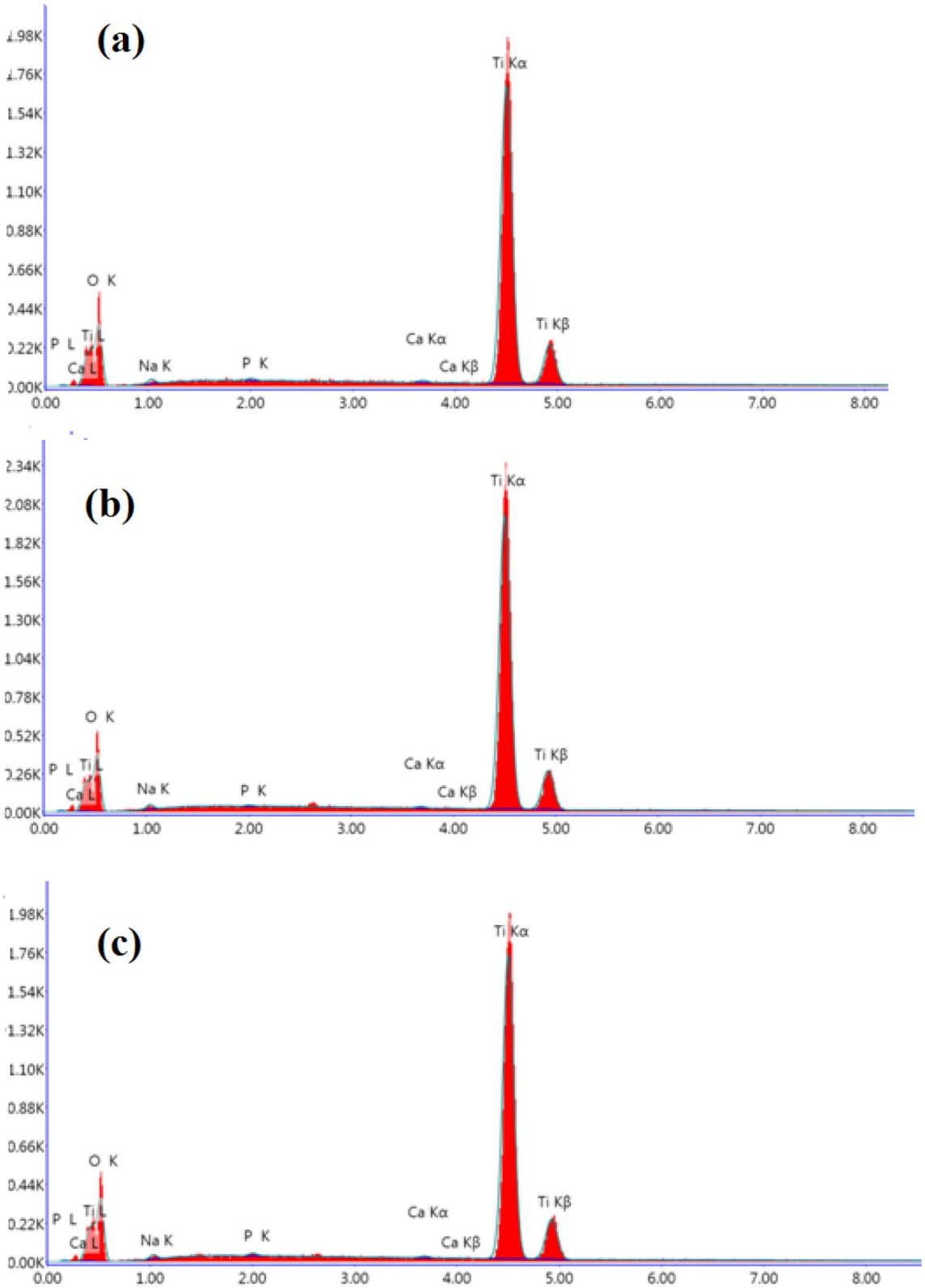

Fig. 3 EDX analysis of anodized /annealed samples **a** 10%, **b** 50% and **c** 70% cry TNTs after immersion in 0.29 g $l^{-1}Ca^{2+}$ for 6 h

Table 2 The composition of cry TNTs surface after immersion in Ca^{2+} at pH 7.4

Glycerol conc (%)	Immersion. time	Wt. %					At. %				
		Ti	O	Ca	P	Na	Ti	O	Ca	P	Na
10	6 h	56.60	41.68	0.26	0.20	1.30	30.65	67.59	0.17	0.18	1.41
50	6 h	57.61	40.45	0.22	0.11	1.40	31.71	66.44	0.15	0.11	1.61
70	6 h	55.98	43.59	0.21	0.22	1.03	30.5	67.82	0.14	0.21	1.32
10	7 day	56.25	39.31	0.46	0.32	2.37	30.96	64.787	0.3	0.28	2.72

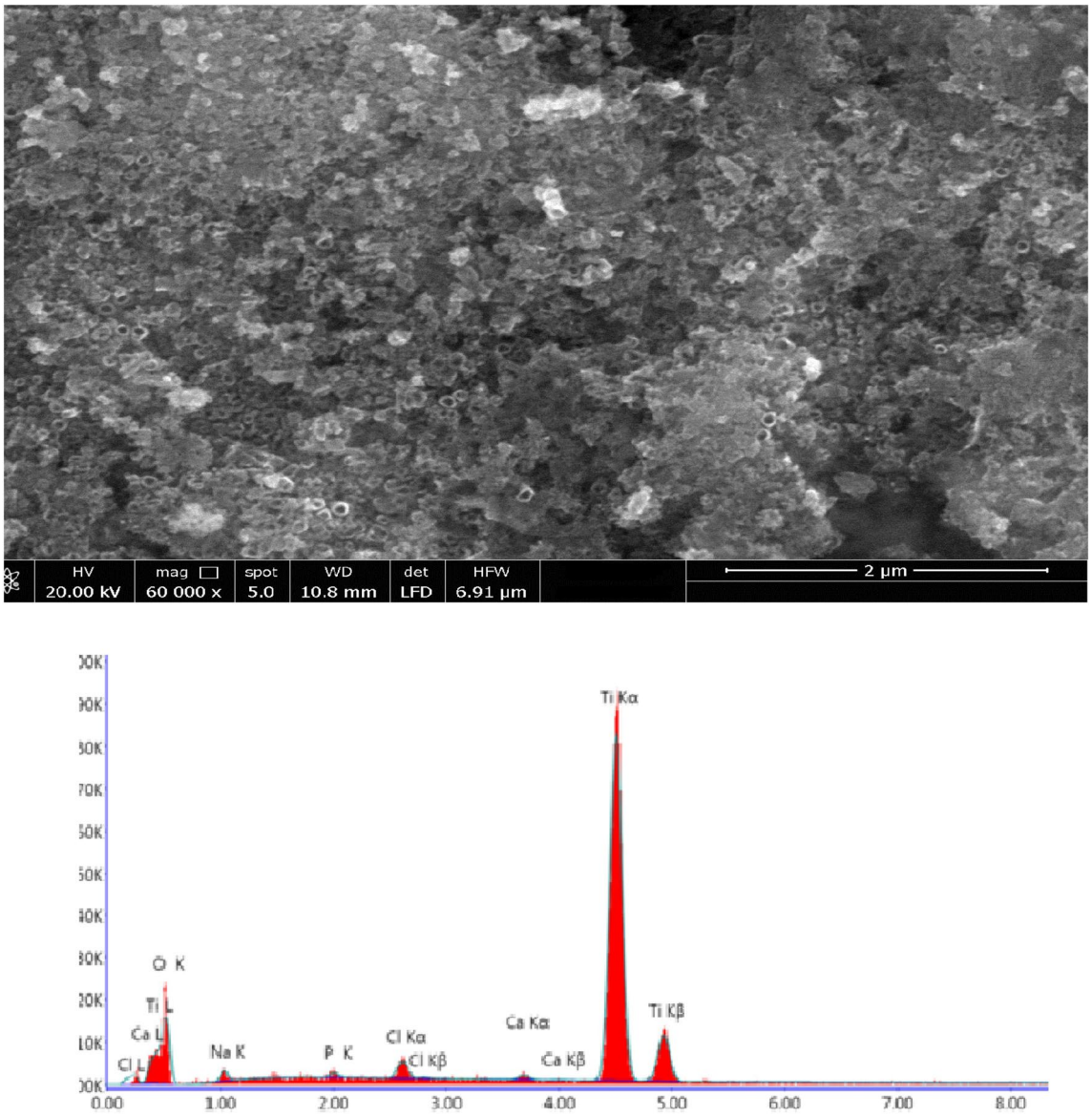

Fig. 4 HR-SEM image and EDX analysis of anodized/annealed sample in 10% cry TNT after immersion in 0.29 g l^{-1} Ca^{2+} solution for 7 days

SBF. On the other side, the OCP of 50% and 70% cry TNTs shifted to negative potential values when they were filled with Ca^{2+} ions, they also shifted to more negative, particularly without Ca^{2+} ions as shown in Fig. 7b. These results indicate that both 50% and 70% of samples have a similar trend unlike that of 10% cry TNT. Furthermore, the incorporation of physiological anions can enhance the bioactive ability of 10% cry TNT in SBF.

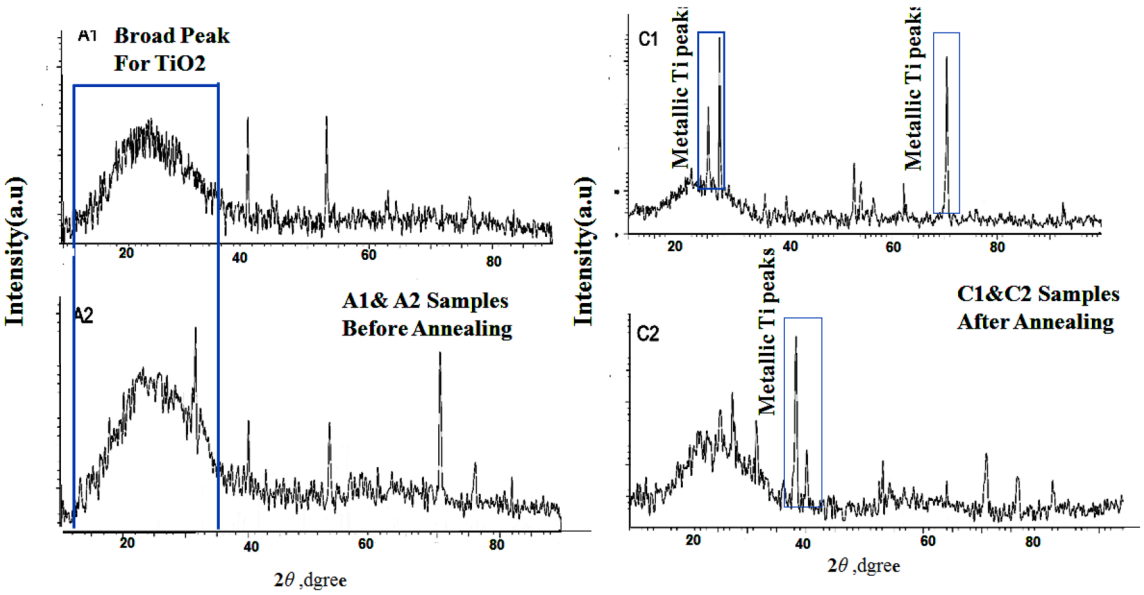

Fig. 5 XRD pattern for anodized Titanium (A1 & C1) and (A2 & C2) anodized Titanium with immersion in 0.29 g l^{-1} Ca^{2+} solution for 6 h

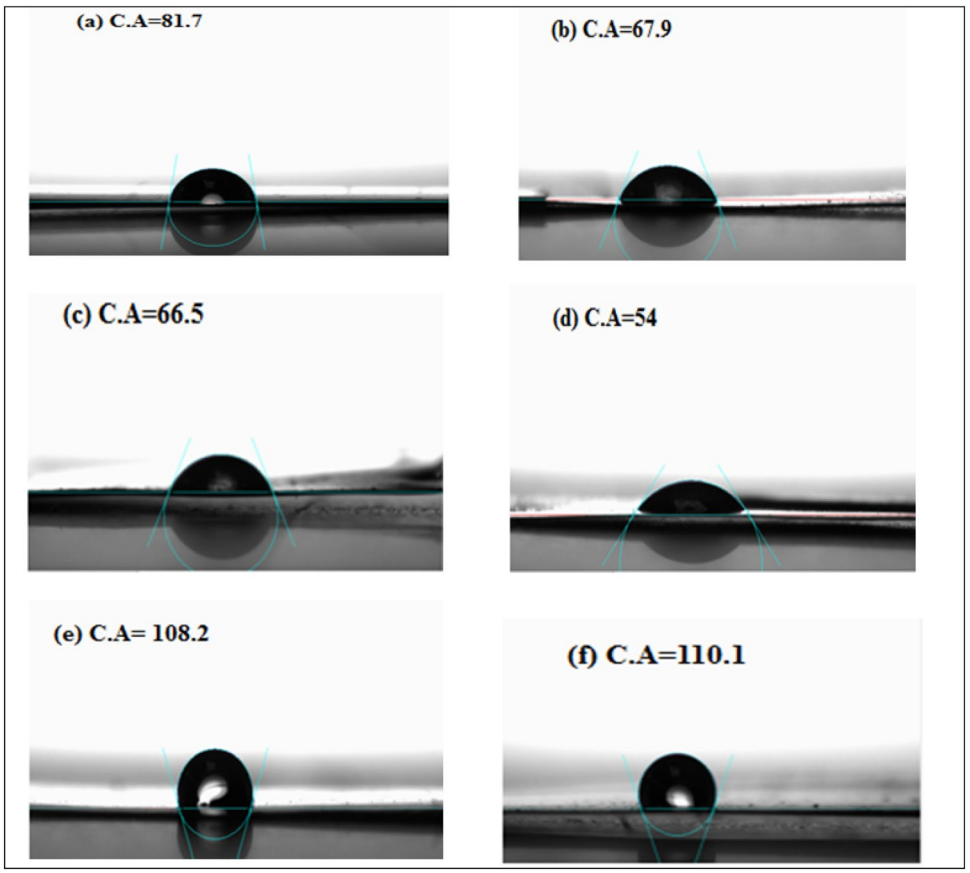

Fig. 6 The value of contact angle (C.A) **a** Ti substrate, **b** anodizes 10% amp Titania, **c** anodized/annealed 10% cry TNT, **d** anodized/annealed10% cry TNT after immersion in 0.29 g l^{-1} Ca^{2+}, **e** anodized/annealed 50% cry TNT, **f** anodized /annealed 70% cry TNT

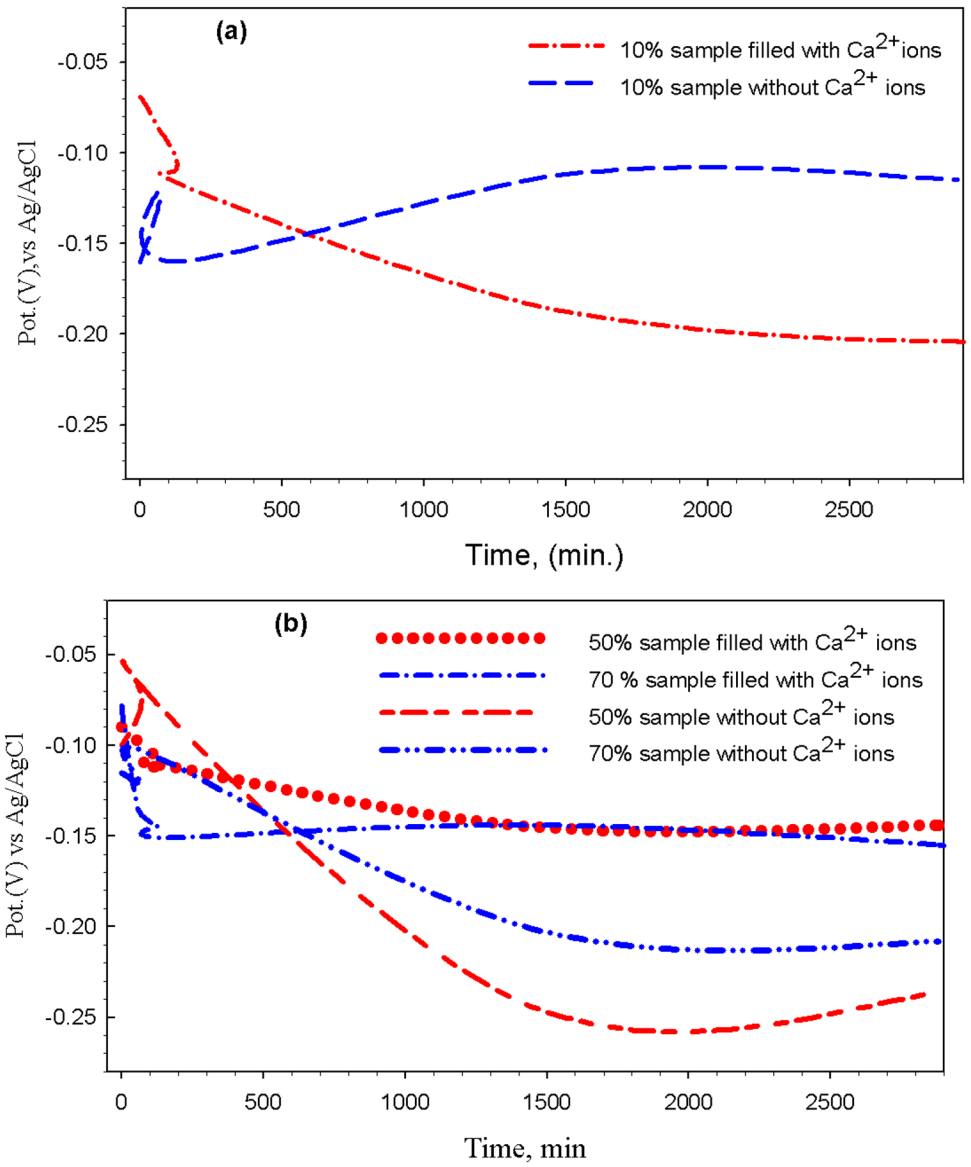

Fig. 7 The variation of OCP with time of 10, 50 and 70% Cry TNTs before and after immersion of 0.29 g $l^{-1}Ca^{2+}$ for 6 h

3.2.2 EIS measurements

To guarantee the whole description of the electrochemical process at the electrode/electrolyte interface on all samples surface, electrochemical impedance spectroscopy (EIS) measurements were made in a wide frequency range after stabilization of the testing samples at the OCP. EIS is one of the most useful non-destructive tools that provide reliable data to evaluate the stability of the passive films by studying charge transfer resistance at a surface/electrolyte interface. The EIS data at open circuit potential of the 10, 50, and 70% cry TNTs with and without Ca^{2+} in SBF solution are presented in the form of Nyquist plots as shown in Fig. 8a–c.

Nyquist plots for all samples show the incomplete semi-circles related to glycerol concentration, this means that stabilization of the passive film in SBF is affected by changing the concentration of glycerol solution [61]. The diameter of the Nyquist plot for the 10% TNT has the highest value, indicating an increase in the resistance and the high dielectric property of the protective passive film. While 70% TNT showed the lowest one with/ and without immersion.

Table 3 Variation of OCP with time of cry TNTs without/and with Ca^{2+}

Cry TNTs (%)	Initial OCP (mV) vs Ag/AgCl		After 48 h OCP (mV) vs Ag/AgCl	
	Without Ca^{2+}	With Ca^{2+}	Without Ca^{2+}	With Ca^{2+}
10	− 160	− 69	− 115	− 204
50	− 100	− 90	− 236	− 144
70	− 115	− 78	− 208	− 155

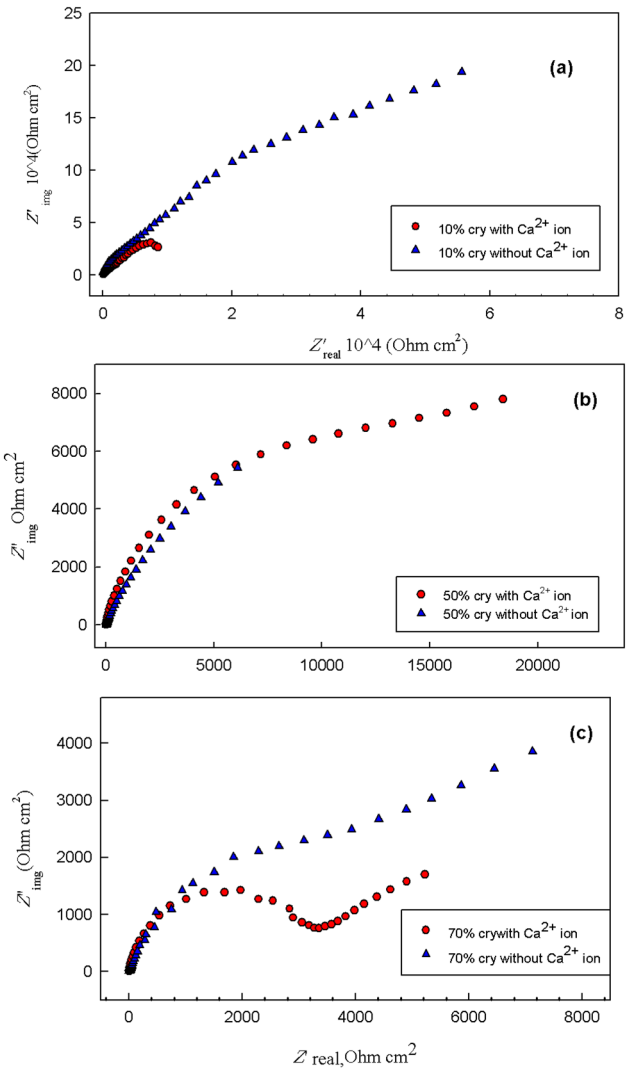

Fig. 8 Nyquist plots of **a** 10%, **b** 50%, **c** 70% cry TNTs before and after immersion in Ca^{2+} ions

The extent of the arc in the Nyquist plot is an indication of relative charge transfer kinetics as shown in Fig. 8a–c [62]. The increase of resistance as can be seen by the diameters of semicircles can be related to the morphological changes than to chemical composition. TiO_2 nanotubes show high electrical resistivity because of their semiconducting nature.

To highlight the role of Ca^{2+} ions and how they can affect the electrochemical behavior of the TNTs, the set of Fig. 8a–c represent the EIS spectra of 10%, 50%, and 70% cry TNTs filled with/ and without Ca^{2+} ions for comparison. The general features of the impedance plots are consistent with passive film behavior especially for 10% TNT, which shows a high impedance diameter over a wide frequency range Fig. 8a.

Once more, it can be noticed that the Ca^{2+} ions which filled the pores of 10% TNT led to decrease its resistance in SBF, this supports the fact, where fewer anions absorption from SBF occur when Ca levels are too high [63] and the OCP results of the present work as shown in Fig. 7a. This result proved that the anodized films play an important role in improving the corrosion resistance in bio-environments solution especially 10% cry TNT highlighting its potency as good passive bioactive surface. Based on Fig. 8b, c it can be confirmed that 50% and 70% TNTs were not considered as good bioactive surfaces, but may be considered as an active surfaces for charge transfer applications.

To illustrate the mechanism of the reaction, which happened at the electrode/ electrolyte interface, the experimental impedance data were fitted to theoretical data according to the proposed model. The slight deviation observed which can be attributed to the high porosity and roughness of the surface on all TNTs. The results of the fitting data for 10, 50, and 70% cry TNTs formed with/ and without Ca^{2+} are presented in Fig. 9a, b. The values of the equivalent circuit parameters for all TNTs are listed in Table 4.

The two-time constant equivalent circuit is presented in Fig. 9c, where the roughness, duplex nature of the passive film, grain border, and bulk/electrolyte interfaces and solution resistance (R_s) were taken into consideration [62]. R_s is in series to two parallel combinations, (R_b & Q_b) representing the inner barrier layer resistance and capacitance, and (R_p & A_{pe}), representing the outer nano-porous layer resistance and capacitance, respectively. The circuit is just one of the possible equivalent circuits that are fit the impedance spectra.

$$Z_{CPE}(\omega) = [Q(j\omega)^n]^{-1}, \tag{3}$$

Q is a constant phase element (CPE), where n varies between 0 and 1 is introduced to explain the deviation from the ideal capacitive behavior due to surface roughness factors and adsorption effects.

Titanium is known to have an active /passive surface in contact with solutions due to the continuous process of dissolution and re-passivation. Thus the composition and the properties of the passive film were changed with the environment. As seen in OCP, the outer layer starts to dissolve and after a certain time, the thickness increases due to adsorption of Ca and P. The change of the outer film capacitance, C_p, can be used as an indicator of the change in the layer thickness. The reciprocal of the capacitance $1/C_p$ is directly proportional to the thickness of this passive layer.

High inner film resistance, R_b of 18.7 KΩ cm^2, and the low capacitance of 3.39 μF cm^{-2} are recorded for 10% TNTs compared to 50% and 70% in case of filled with Ca^{2+} ions as shown in Fig. 9a, b and Table 4. This result also supports previous findings that a 10% cry TNT has distinct properties more than that of 50% and 70% in SBF. On the other hand, the values of porous layers resistant R_p increases reaching

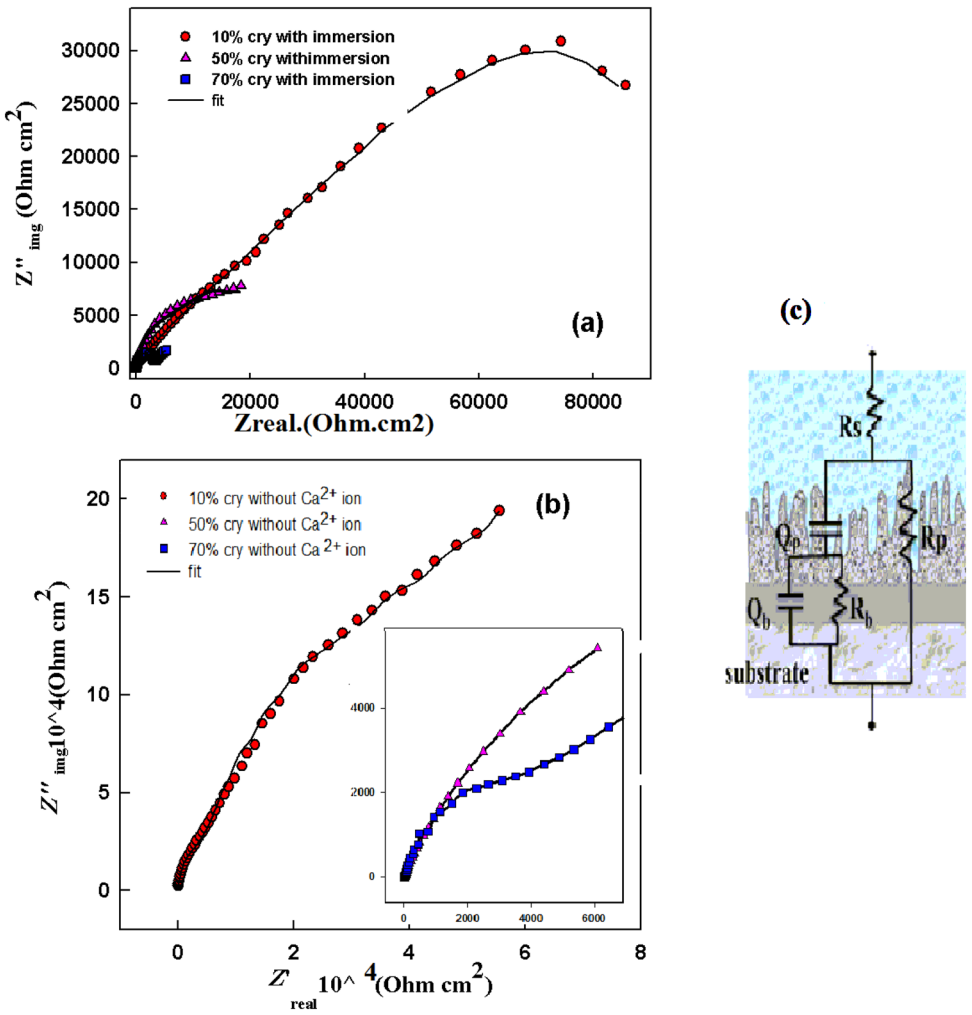

Fig. 9 The fitting curves of the experimental to theoretical data for all samples **a** with immersion in Ca^{2+}, **b** without immersion and **c** the equivalent circuit

Table 4 EIS parameters of cry TNTs with /and without Ca^{2+} ions immersed in SBF at 37° C for 7 days after fitting the EIS plots with equivalent circuit shown in Fig. 9

Electrode (%)	Ca^{2+}	RS (Ω)	Rb (kΩ cm^2)	(CPE)b (μF cm^{-2})	*n*	Rp (kΩ cm^2)	(CPE)p (μF cm^{-2})	*n*
10	Without	11.0	110	6.25	0.9	78.6	2.37	0.44
	With	22.8	18.7	3.39	0.44	118	5.54	0.55
50	Without	5.20	1.0	968	0.23	13	102.9	0.75
	With	9.88	6.12	10.9	0.88	19.21	42.9	0.78
70	Without	2.20	11	13	0.85	10.80	83.8	0.68
	With	5.80	9.74	342	0.53	2.79	2.86	0.90

118.18 KΩ cm^2 for 10% cry TNT compared to 50% and 70%. All the above results can be attributed to the high stability of the film formed on 10% cry TNT in comparison with that formed on 50% and 70% cry TNTs.

Thinning of the oxide film was noticed and proved through low R_p and high Q_p values, for 50% and 70% compared with 10%, and all values were given in detail in Table 4. Instead, Ca^{2+} ions increase the resistance of the outer layer R_p for a 10% sample more than the inner layer. This can be explained as the high incorporation of other ions from the SBF solution into this layer even in the presence of Ca^{2+} ions.

Solution resistance value R_s varied from 5.2 Ω cm^2 to 22.8 Ω cm^2 (see Table 4) it was noticed that R_s for SBF with Ca^{2+} ion higher than without Ca^{2+}. 10% cry TNT with or without Ca^{2+} higher value compared to 50% and 70% that showed slow incorporation of ions into the infra-nano structure of these samples compared with a 10%. These results are indicated that the TNT formed with 10% glycerol can be considered as an excellent support for the biomimetic Ca–P

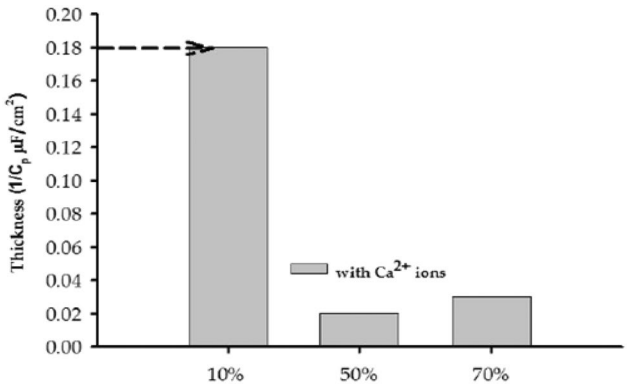

Fig. 10 Variation of the thickness of Titania layer with the glycerol concentrations of 10, 50, and 70% samples after immersion in 0.29 g l^{-1} Ca^{2+} solution for 6 h

layer and can successfully be used as a bioactive surface similar to other our previous reported surfaces [62].

Figure 10 displays that, the reduction of C_p is consistent with the thickness growth of the outer layer for 10% samples filled with/and without Ca^{2+} ions due to the excellent interaction of this surface with the electrolyte in simulated physiological solution which refer to good in-vitro biocompatibility. Similarly, it is clear that a thick passive layer is formed without Ca^{2+} ions on a 10% TNT, while a thin layer is formed on 50% and 70% samples with/and without Ca^{2+} ions.

The decrease of thickness is due to, the rise of Ca^{2+} ions inside the tube resulted in adsorption of negatively charged ions from the SBF as phosphorus ions increase until it reaches a constant value and vice versa [59]. Consequently, the Ca^{2+} ions are responsible for the resistance elevation [49]. The film thickness of the TNT on 10% sample through the formation of Ca–P coating layer (with ratio equal to1.3 after 6 h and 1.47 after 7 days of immersion in SBF) indicates the adsorption of SBF. It could be seen that R_p is much higher than R_b, and the highest value of R_b for the 10% TNT was reported without immersion in Ca^{2+} ions indicated that the inner layer was porous and compact [57]. R_p value increased with Ca^{2+} ions immersion. The high value of R_p confirmed the formation of high corrosion protection layer due to the increase in the film coverage and thickness, which is in agreement with the results of SEM analysis as shown in Figs. 1 and 2.

Finally, Nyquist plot of 70% TNT filled with Ca^{2+} ions exhibits more interesting result, where it was found to consist of two parts, a semicircle at high and intermediate frequencies with very small diameter and a linear part at low frequencies as shown in Fig. 8c, this result assures that 70% sample act as a promising candidate for further studies to use it for energy and sensing applications rather than orthopedic applications.

4 Conclusion

The goal of this work falls into three categories: surface modification, film resistance, and biocompatibility analysis. This study provides a new understanding of the factors accelerating the bioactivity of Ti metal during various chemical and thermal treatments to design and fabricate innovative surfaces with high biocompatibility and bonding ability for dental and orthopedic applications. This protocol of anodization in fluorinated glycerol electrolyte on titanium under two sequential potential steps produced a novel platform highly ordered nanotubes structure from Titania with a wide range of pore sizes. Cry TNTs formed after heat treatment are the most efficient phase for good wettability properties with a 54° contact angle. This study confirmed that the concentration of glycerol of more than 10% decreases the bioactivity of the Titania surface. Also, TNT improves Ca^{2+} ions incorporation into the porous structure that affects positively its wettability properties. Moreover, Ca^{2+} ions enhance the resistance of 10% cry TNT from 78 to 118 kΩ in SBF. 70% cry TNT showed promising EIS plots to be used for future applications related to energy and sensing.

Acknowledgements The authors wish to acknowledge the National Research Centre (NRC) for financial support to this work as a part of the Grant (AR111905).

Declarations

Conflict of interest The author declares that there are no conflicts of interest.

References

1. Fadl-allah SA, Mohsen Q, El-Shenawy NS (2011) Stainless steel implantation-induced changes in surface characteristics, corrosion resistance, and hemato-biochemical parameters of male rat. J Am Sci 7:84–91
2. Liu X, Chu PK, Ding C (2004) Surface modification of titanium, titanium alloys, and related materials for biomedical applications. Mater Sci Eng R 47:49–121
3. Bose S, Banerjee D, Shivaram A, Tarafder S, Bandyopadhyay A (2018) Calcium phosphate coated 3D printed porous titanium with nanoscale surface modification for orthopedic and dental applications. Mater Des 151:102–112
4. Domínguez-Trujillo C, Ternero F, Rodríguez-Ortiz JA, Heise S, Boccaccini AR, Lebrato J, Torres Y (2018) Bioactive coatings on porous titanium for biomedical applications. Surf Coat Technol 349:584–592
5. Stern JK, Hahn EE, Evian CI, Waasdorp J, Rosenberg ES (2015) Implant failure: prevalence, risk factors, management, and prevention. In: Dental implant complications: etiology, prevention, and treatment, vol 2. Wiley, pp 153–169
6. Torres DL, Pereira MC, Silva JWJ, Codaro EN, Acciari HA (2015) Effect of phosphoric acid concentration and anodizing time

on the properties of anodic films on titanium. J Eng Sci Technol 10:841–848
7. Kang KW, Limandri S, Castellano G, Suárez S, Trincavelli J (2017) Thickness determination of anodic titanium oxide films by electron probe microanalysis. Mater Charact 130:50–55
8. Bauer S, Park J, von der Mark K, Schmuki P (2008) Improved attachment of mesenchymal stem cells on super-hydrophobic TiO2 nanotubes. Acta Biomater 4:1576–1582
9. Macak JM, Tsuchiya H, Taveira L, Ghicov A, Schmuki P (2005) Self-organized nanotubular oxide layers on Ti-6Al-7Nb and Ti-6Al-4V formed by anodization in NH4F solutions. J Biomed Mater Res Part A 75:928–933
10. Patel SB, Hamlekhan A, Royhman D, Butt A, Yuan J, Shokuhfar T, Sukotjo C, Mathew MT, Jursich G, Takoudis CG (2014) Enhancing surface characteristics of Ti–6Al–4V for bio-implants using integrated anodization and thermal oxidation. J Mater Chem B 2:3597–3608
11. Shah, A., Ismail, S. N. F., Hassam, M. A., and Daud, R. (2018) Surface modification on titanium alloy for biomedical application, Beddows C reference module in Materials Science and Materials Engineering. Elsevier, Amsterdam pp 1–9.
12. Su Z, Zhou W (2011) Formation, morphology control and applications of anodic TiO_2 nanotube arrays. J Mater Chem 21:8955–8970
13. Sun Y-S, Liu J-F, Wu C-P, Huang H-H (2015) Nanoporous surface topography enhances bone cell differentiation on Ti–6Al–7Nb alloy in bone implant applications. J Alloys Compd 643:S124–S132
14. Das K, Bandyopadhyay A, Bose S (2008) Biocompatibility and in situ growth of TiO_2 nanotubes on Ti using different electrolyte chemistry. J Am Ceram Soc 91:2808–2814
15. Yao C, Webster TJ (2006) Anodization: a promising nano-modification technique of titanium implants for orthopedic applications. J Nanosci Nanotechnol 6:2682–2692
16. Melghit K, Bouziane K (2008) Room temperature ferromagnetism of iron-doped rutile TiO_2 nanorods synthesized by a low temperature method. J Alloys Compd 453:102–107
17. Lin Y (2008) Photocatalytic activity of TiO_2 nanowire arrays. Mater Lett 62:1246–1248
18. Fang D, Huang K, Liu S, Li Z (2008) Electrochemical properties of ordered TiO_2 nanotube loaded with Ag nano-particles for lithium anode material. J Alloys Compd 464:L5–L9
19. Sharifi T, Ghayeb Y, Mohammadi T, Momeni MM, Bagheri R, Song Z (2021) Surface treatment of titanium by in-situ anodizination and NiO photodeposition: enhancement of photoelectrochemical properties for water splitting and photocathodic protection of stainless steel. Appl Phys A 127:1–12
20. Momeni MM, Akbarnia M, Ghayeb Y (2020) Preparation of S-W-codoped TiO2 nanotubes and effect of various hole scavengers on their photoelectrochemical activity: alcohol series. Int J Hydrogen Energy 45:33552–33562
21. Gong D, Grimes CA, Varghese OK, Hu W, Singh RS, Chen Z, Dickey EC (2001) Titanium oxide nanotube arrays prepared by anodic oxidation. J Mater Res 16:3331–3334
22. Momeni MM, Hosseini MG (2014) Different TiO_2 nanotubes for back illuminated dye sensitized solar cell: fabrication, characterization and electrochemical impedance properties of DSSCs. J Mater Sci 25:5027–5034
23. Beranek R, Hildebrand H, Schmuki P (2003) Self-organized porous titanium oxide prepared in H_2SO_4/HF electrolytes. Electrochem Solid State Lett 6:B12
24. Macak JM, Sirotna K, Schmuki P (2005) Self-organized porous titanium oxide prepared in Na_2SO_4/NaF electrolytes. Electrochim Acta 50:3679–3684
25. Momeni MM, Hakimian M, Kazempour A (2016) Preparation and characterisation of manganese–TiO_2 nanocomposites for solar water splitting. Surf Eng 32:514–519
26. Acciari HA, Palma DPS, Codaro EN, Zhou Q, Wang J, Ling Y, Zhang J, Zhang Z (2019) Surface modifications by both anodic oxidation and ion beam implantation on electropolished titanium substrates. Appl Surf Sci 487:1111–1120
27. Hatamleh MM, Wu X, Alnazzawi A, Watson J, Watts D (2018) Surface characteristics and biocompatibility of cranioplasty titanium implants following different surface treatments. Dent Mater 34:676–683
28. Klein MO, Bijelic A, Ziebart T, Koch F, Kämmerer PW, Wieland M, Konerding MA, Al-Nawas B (2013) Submicron scale-structured hydrophilic titanium surfaces promote early osteogenic gene response for cell adhesion and cell differentiation. Clin Implant Dent Relat Res 15:166–175
29. Rabe M, Verdes D, Seeger S (2011) Understanding protein adsorption phenomena at solid surfaces. Adv Coll Interface Sci 162:87–106
30. Mavrogenis AF, Dimitriou R, Parvizi J, Babis GC (2009) Biology of implant osseointegration. J Musculoskelet Neuronal Interact 9:61–71
31. Sun Y-S, Huang H-H (2018) Biphasic calcium phosphates/tantalum pentoxide hybrid layer and its effects on corrosion resistance and biocompatibility of titanium surface for orthopedic implant applications. J Alloys Compd 743:99–107
32. Biggs MJP, Richards RG, Gadegaard N, McMurray RJ, Affrossman S, Wilkinson CDW, Oreffo ROC, Dalby MJ (2009) Interactions with nanoscale topography: adhesion quantification and signal transduction in cells of osteogenic and multipotent lineage. J Biomed Mater Res Part A 91:195–208
33. Dalby MJ, McCloy D, Robertson M, Wilkinson CDW, Oreffo ROC (2006) Osteoprogenitor response to defined topographies with nanoscale depths. Biomaterials 27:1306–1315
34. Bierbaum S, Mulansky S, Bognár E, Kientzl I, Nagy P, Vrana NE, Weszl M, Boschke E, Scharnweber D, Wolf-Brandstetter C (2018) Osteogenic nanostructured titanium surfaces with antibacterial properties under conditions that mimic the dynamic situation in the oral cavity. Biomater Sci 6:1390–1402
35. He WEI, Gonsalves KE, Halberstadt CR (2007) Micro/nanomachining and fabrication of materials for biomedical applications. Biomed Nanostruct 40:25–47
36. Park IS, Oh HJ, Bae TS (2013) Bioactivity and generation of anodized nanotubular TiO_2 layer of Ti–6Al–4V alloy in glycerol solution. Thin Solid Films 548:292–298
37. Allam NK, Grimes CA (2007) Formation of vertically oriented TiO2 nanotube arrays using a fluoride free HCl aqueous electrolyte. J Phys Chem C 111:13028–13032
38. Minagar S, Berndt CC, Wang J, Ivanova E, Wen C (2012) A review of the application of anodization for the fabrication of nanotubes on metal implant surfaces. Acta Biomater 8:2875–2888
39. Abdel-Karim AM, Salama AH, El-Samahy FA, El-Sedik M, Osman FH (2017) Some dielectric properties of novel nano-s-triazine derivatives. J Phys Org Chem 30:3703
40. Kokubo T, Takadama H (2006) How useful is SBF in predicting in vivo bone bioactivity? Biomaterials 27:2907–2915
41. Kunze J, Seyeux A, Schmuki P (2007) Anodic TiO_2 layer conversion: fluoride-induced rutile formation at room temperature. Electrochem Solid State Lett 11:K11
42. Rani S, Roy SC, Paulose M, Varghese OK, Mor GK, Kim S, Yoriya S, LaTempa TJ, Grimes CA (2010) Synthesis and applications of electrochemically self-assembled titania nanotube arrays. Phys Chem Chem Phys 12:2780–2800

43. Liu G, Wang K, Hoivik N, Jakobsen H (2012) Progress on free-standing and flow-through TiO_2 nanotube membranes. Sol Energy Mater Sol Cells 98:24–38
44. Joseph S, Sagayaraj P (2015) A cost effective approach for developing substrate stable TiO_2 nanotube arrays with tuned morphology: a comprehensive study on the role of H_2O_2 and anodization potential. New J Chem 39:5402–5409
45. Kulkarni M, Mazare A, Schmuki P, Iglič A (2014) Biomaterial surface modification of titanium and titanium alloys for medical applications. Nanomedicine 111:111
46. Raja KS, Misra M, Paramguru K (2005) Formation of self-ordered nano-tubular structure of anodic oxide layer on titanium. Electrochim Acta 51:154–165
47. Liang H-C, Li X-Z (2009) Effects of structure of anodic TiO_2 nanotube arrays on photocatalytic activity for the degradation of 2, 3-dichlorophenol in aqueous solution. J Hazard Mater 162:1415–1422
48. Fadl-allah SA, Mohsen Q (2010) Characterization of native and anodic oxide films formed on commercial pure titanium using electrochemical properties and morphology techniques. Appl Surf Sci 256:5849–5855
49. Narayanan R, Lee H-J, Kwon T-Y, Kim K-H (2011) Anodic TiO2 nanotubes from stirred baths: hydroxyapatite growth & osteoblast responses. Mater Chem Phys 125:510–517
50. Fathi AM, Shehata OS, Abdel-Karim AM (2019) The photoactivity and electrochemical behavior of porous titania (TiO_2) in simulated saliva for dental implant application. SILICON 11:2353–2363
51. Chen X-B, Li Y-C, Du Plessis J, Hodgson PD (2009) Influence of calcium ion deposition on apatite-inducing ability of porous titanium for biomedical applications. Acta Biomater 5:1808–1820
52. El-Rab SMFG, Fadl-allah SA, Montser AA (2012) Improvement in antibacterial properties of Ti by electrodeposition of biomimetic Ca–P apatite coat on anodized titania. Appl Surf Sci 261:1–7
53. Yang G-l, He F-M, Song E, Hu J-A, Wang X-X, Zhao S-F (2010) In vivo comparison of bone formation on titanium implant surfaces coated with biomimetically deposited calcium phosphate or electrochemically deposited hydroxyapatite. Int J Oral Maxillofac Implants 25:12
54. Kouhi M, Prabhakaran MP, Shamanian M, Fathi M, Morshed M, Ramakrishna S (2015) Electrospun PHBV nanofibers containing HA and bredigite nanoparticles: fabrication, characterization and evaluation of mechanical properties and bioactivity. Compos Sci Technol 121:115–122
55. Allam NK, Grimes CA (2009) Effect of rapid infrared annealing on the photoelectrochemical properties of anodically fabricated TiO_2 nanotube arrays. J Phys Chem C 113:7996–7999
56. Yoriya S, Kittimeteeworakul W, Punprasert N (2012) Effect of anodization parameters on morphologies of TiO2 nanotube arrays and their surface properties. J Chem Chem Eng 6:686
57. Dikici T, Erol M, Toparli M, Çelik E (2014) Characterization and photocatalytic properties of nanoporous titanium dioxide layer fabricated on pure titanium substrates by the anodic oxidation process. Ceram Int 40:1587–1591
58. Slimen H, Houas A, Nogier JP (2011) Elaboration of stable anatase TiO_2 through activated carbon addition with high photocatalytic activity under visible light. J Photochem Photobiol A 221:13–21
59. Schwarz F, Ferrari D, Herten M, Mihatovic I, Wieland M, Sager M, Becker J (2007) Effects of surface hydrophilicity and microtopography on early stages of soft and hard tissue integration at non-submerged titanium implants: an immunohistochemical study in dogs. J Periodontol 78:2171–2184
60. Prakash CGJ, Raj CC, Prasanth R (2017) Fabrication of zero contact angle ultra-super hydrophilic surfaces. J Colloid Interface Sci 496:300–310
61. Vasilescu C, Drob SI, Moreno JMC, Osiceanu P, Popa M, Vasilescu E, Marcu M, Drob P (2015) Long-term corrosion resistance of new Ti–Ta–Zr alloy in simulated physiological fluids by electrochemical and surface analysis methods. Corros Sci 93:310–323
62. Mohsen Q, Fadl-Allah SA, El-Shenawy NS (2012) Electrochemical impedance spectroscopy study of the adsorption behavior of bovine serum albumin at biomimetic calcium–phosphate coating. Int J Electrochem Sci 7:4510–4527
63. Kar A, Raja KS, Misra M (2006) Electrodeposition of hydroxyapatite onto nanotubular TiO_2 for implant applications. Surf Coat Technol 201:3723–3731